Hu Z, Gallacher B.

A mode-matched force-rebalance control for a MEMS vibratory gyroscope.

***Sensors & Actuators: A. Physical* 2018, 273, 1-11.**

A Mode-Matched Force-Rebalance Control for a MEMS Vibratory Gyroscope

Zhongxu Hu, Barry Gallacher

School of Mechanical and System Engineering, Newcastle University, Newcastle upon Tyne, UK

Abstract

The force-to-rebalance (FTR) closed-loop control is widely used in MEMS vibratory gyroscopes. However, most of these applications may operate in split modes, as mode matching is usually conducted open loop. There is a lack of discussion explicitly addressing the significance of mode matching in the FTR operation mode. This paper investigates the influence of mode mistuning on the FTR closed-loop control of a MEMS Coriolis vibratory gyroscope (CVG), and proposes a novel tuning method using real time control forces to achieve a mode-matched FTR control. The analysis and design of the FTR is based on the time averaged equations of motion, where the sense mode vibration is decomposed into the quadrature and in-phase channels with cross coupling determined by the frequency mismatch between the drive and sense modes of vibration. The control design is treated as a 2x2 multivariable control problem using the individual channel design (ICD) framework. Independent control design for each of the two channels allows the bandwidth of the quadrature loop to be significantly less than the in-phase loop. The characteristics of mode mistuning can be extracted from the real time feedback forces. Using this information, the desirable mode-matched uncoupled FTR can be implemented. The FTR closed-loop control eliminates the influences of frequency mismatch on the zero rate output and linearity of the scale factor. It therefore relaxes the degree to which the modes need to be tuned. It is shown in this study that matching the modes in the FTR control scheme improves noise performance and measurement accuracy over the non-tuned case. Experimental results of real time FTR control and Allan deviation tests are provided to verify the analysis.

Keywords: Coriolis vibratory gyroscope, Mode matching, Force rebalance control, Individual channel design

1. Introduction

The principle of MEMS CVGs is based on energy transfer between a pair of degenerate vibration modes due to Coriolis coupling in the presence of rate input. Degenerate modes exist in cyclically symmetric structures. Gyroscope design utilising disks, rings, and hemispheric shells [1][2][3][4][5] or common due to the inherent mode matching caused by degeneracy. For rate mode CVGs, the primary mode is excited into resonance with a constant amplitude of vibration controlled by a phase locked loop (PLL) and an automatic gain control (AGC). When the gyroscope is operated in open-loop mode, the amplitude and phase of vibration of the sense mode excited by Coriolis force are used to calculate the rate of rotation. A large amplitude of vibration of the drive mode is desirable for increasing the scale factor and consequently the signal-to-noise ratio (SNR) and bias stability. In order to improve the sensitivity of the electrostatic transducer, high DC bias, smaller capacitive gaps and bigger capacitive areas in the design of the resonant structure are also desirable.

A high quality factor of the resonator results in low power consumption, lower noise floor and improved mechanical amplification of the response to Coriolis action. Most gyroscopes operates at the resonance frequency of the drive mode. This makes mode matching vital for high performance gyroscopes as it increases the mechanical amplification quality of the sense mode which in turn improves key performances metrics. Mode alignment and frequency matching are often implemented and verified open loop. Using this approach results in mode matching to the order of mHz [5][6][7]. A disadvantage of this open loop approach is that the mode matched state is not independent of the external rate. External rate perturbs the mode frequencies. Furthermore, mechanical and electrostatic nonlinearities result in coupling between the amplitude and frequency of the response. It is therefore practically impossible to maintain exact frequency matching of the modes in open loop operation unless the applied rate is highly restricted. Open loop operation of CVGs are limited to low rate applications such as gyrocompasses and inclinometer where the effect of the rate of the mode frequencies is small.

FTR close-loop control, where the vibration of the sense mode is suppressed, and the rate is calculated from the rebalance forces, is widely used in most practical MEMS CVGs. This closed-loop mode of operation has great advantages over open loop operation, including increased dynamic range, improved scale factor linearity, increased bandwidth of measurement and insensitivity to variation of the Quality factor variation. FTR close-loop control largely eliminates the influences of frequency mismatch on zero rate output (ZRO) and the linearity of scale factor. Therefore, it mitigates the challenge in mode tuning in the post processing of the gyroscope device, and relaxes fabrication tolerance.

Over the years, different forms of force feedback control have been developed for MEMS CVGs, including sigma-delta modulator loops [8], adaptive control [9], robust control [10], and $H\infty$ controller [11]. These methods face challenges due to poor robustness, and requiring complex circuitry, wideband data acquisition and intense computation in the implementation. The most common form of FTR control [12][13] consists of two separate closed-loops with high gains, respectively designed for nulling the in-phase and quadrature components of vibration of the sense mode. This separation allows for independent control design for each of the two channels, for example, the bandwidth of the quadrature loop can be significantly less than the in-phase loop. This is because the quadrature loop only deals with slow time-varying stiffness cross coupling, while the in-phase loop needs to counteract the fast time varying Coriolis force related to the specified measurement bandwidth of the gyro sensor. Though FTR control makes frequency matching less significant to the sensor performance, in mode-split FTR control, the frequency split causes coupling between the in-phase and quadrature nulling loops. This coupling complicates the control design and adversely affects sensor performance. Ideally, mode tuning should be conducted in close-loop operation as it avoids the influences from external rate and the complex interactions between the drive and sense modes of vibration present in open loop operation. Several reports are available in the literature available on the design of FTR from the control theory perspective [14][15][16]. However, few publications discuss the influence of channel coupling on the FTR control performance when applied to the matched-mode and split-mode configurations. In this paper the FTR control design for the split-mode case will be developed. The aim is to understand how the frequency mismatch related control coupling affects the bandwidth, passband errors, the required control gains, robustness of control and eventually the noise performance of the gyro sensor. Further, we propose to tune the modes of a CVG in the close-loop mode using the real time control outputs, to remove the undesirable control coupling. Finally, we show matched-mode to be superior to split-mode for FTR controlled CVGs in terms of noise performance.

The paper is organized as follows. Section 2 introduces the dynamic model, the time averaged equations of motion of CVGs, and the separation of the quadrature and in-phase channels. Section 3 describes a decentralized FTR control design based on the ICD framework[18][19][20], which allows direct use of the frequency domain Bode techniques to each of the quadrature and in-phase channels even though there is strong coupling between them. Section 4 illustrates how mode tuning can be conducted in closed-loop control by extracting information of mode mistuning from the real time rebalance forces. Section 5 provides experimental results to show the benefits of matched modes for FTR control, mainly in noise performance and bias stability.

2. Averaged model of CVGs

This section introduces the dynamic model and the time averaged equations of motion of a CVG with FTR closed-loop control. Close-loop operation effectively avoids interaction between the drive and sense modes of vibration, so that the design of the rebalance control for the sense mode can be independently treated. External forces applied to the sense mode, including stiffness cross coupling and Coriolis coupling, are seen as external disturbances. Loveday in [13] used the averaged model for closed-loop control of CVGs, but no quantitative analysis and control design involving frequency mistuning were provided.

2.1 Dynamic model of CVGs with FTR control

A Coriolis vibratory gyroscope is commonly modeled as a two dimensional oscillator with damping and stiffness couplings. The non-dimensionalized equations of motion of the vibration are described as:

$$\ddot{x} + d_{xx}\dot{x} + d_{xy}\dot{y} + {\omega_x}^2\, x + k_{xy}y = \quad 2\Omega\dot{y} + F_x \tag{1}$$

$$\ddot{y} + d_{yx}\dot{x} + d_{yy}\dot{y} + k_{yx}x + {\omega_y}^2\, y = -2\Omega\dot{x} + F_y \tag{2}$$

Where x and y are the displacement of vibration, d_{xx} and d_{yy} are the damping coefficients, ω_x and ω_y are the natural frequencies of the drive and sense axes respectively. The terms d_{xy}, d_{yx} and k_{xy}, k_{yx} represent the non-ideal damping and stiffness cross couplings between the resonators. The term Ω is the external rate input that induces the Coriolis coupling. F_x and F_y are electrostatic forces, to excite the drive mode into resonance with a specified constant amplitude and to null the sense mode in response to the quadrature and Coriolis forces.

When the gyroscope is operated in rate mode, the sinusoidal drive force $F_x = F\sin\omega_x t$ excites the drive mode into resonance with a constant amplitude A_x. The displacement and velocity of vibration of the drive mode can be expressed as $x = -A_x\cos\omega_x t$, and $\dot{x} = \omega_x A_x \sin\omega_x t$. The motion of vibration of the sense mode is governed by:

$$\ddot{y} + d_{yy}\dot{y} + {\omega_y}^2\, y = -2\Omega\dot{x} - d_{yx}\dot{x} - k_{yx}x + F_y \tag{3}$$

When the gyroscope is operated in closed-loop mode, the rebalance force F_y cancels all the external forces acting on the sense mode. When the force rebalance control reaches steady state, vibration of the sense mode is completely suppressed, so that $y = \dot{y} = \ddot{y} = 0$, the required rebalance force F_y is given by:

$$F_y = 2\Omega\dot{x} + d_{yx}\dot{x} + k_{yx}x \tag{4}$$

It can be decomposed into two orthogonal forces, the quadrature and in-phase components:

$$F_{ys} = \left(2\Omega + d_{yx}\right)\omega_x A_x \sin\ \omega_x t \tag{5}$$

$$F_{yc} = k_{yx}A_x \cos\ \omega_x t \tag{6}$$

The force F_{ys} that is in-phase with the excitation of the drive mode is used as a measure of rotation rate. Note that the damping imperfection causes a small zero rate output (ZRO) since $d_{yx} \ll \Omega$. Quadrature force F_{yc} reflects the elastic mode coupling k_{yx}. From equation (5) and after subsequent demodulation the scale factor (SF) defined as F_{ys}/Ω is given by $= 2\omega_x A_x$. The ZRO can be defined from equation (5) as $= d_{yx}\ \omega_x A_x$. The scale factor SF is independent of both the frequency split, defined as $\Delta\omega = \omega_x - \omega_y$, and the Q-factor. This is a major advantage of the FTR approach.

2.2 Averaged model

The analysis and design of FTR control may be more convenient based on the reduced order time-averaged model of CVGs [12][13][17]. The time averaged model avoids the fast time varying harmonic vibration, only deals with the slow time varying amplitude and phase variables, which allows easier implementation using low cost and low speed hardware platforms. Relative to the reference phase, the rebalance control forces are synthesized conveniently by using two orthogonal signals $\sin\omega t$ and $\cos\omega t$ by:

$$\begin{cases} F_x = F_{xs}\sin\omega t + F_{xc}\cos\omega t \\ F_y = F_{ys}\sin\omega t + F_{yc}\cos\omega t \end{cases} \tag{7}$$

Fast time-varying displacement of vibration signals are expressed using the in-phase and quadrature components, C_x, S_x, C_y, S_y, which are slow time-varying variables:

$$\begin{cases} x(t) = C_x(t)\sin\omega t + S_x(t)\cos\omega t \\ y(t) = C_y(t)\sin\omega t + S_y(t)\cos\omega t \end{cases} \tag{8}$$

The well-known averaging process assumes the slow-varying parameters are constant during one period of vibration [13][21]. The resulting equations of motion of the envelope variables without explicit involvement of time are:

$$\dot{S}_x = -\frac{d_{xx}}{2}S_x - \frac{{\omega_x}^2-\omega^2}{2\omega}C_x - \frac{d_{xy}-2\Omega}{2}S_y - \frac{k_{xy}}{2\omega}C_y + \frac{1}{2\omega}F_{xc} \quad (9)$$

$$\dot{C}_x = \frac{{\omega_x}^2-\omega^2}{2\omega}S_x - \frac{d_{xx}}{2}C_x + \frac{k_{xy}}{2\omega}S_y - \frac{d_{xy}-2\Omega}{2}C_y - \frac{1}{2\omega}F_{xs} \quad (10)$$

$$\dot{S}_y = -\frac{d_{yx}+2\Omega}{2}S_x - \frac{k_{yx}}{2\omega}C_x - \frac{d_{yy}}{2}S_y - \frac{{\omega_y}^2-\omega^2}{2\omega}C_y + \frac{1}{2\omega}F_{yc} \quad (11)$$

$$\dot{C}_y = \frac{k_{yx}}{2\omega}S_x - \frac{d_{yx}+2\Omega}{2}C_x + \frac{{\omega_y}^2-\omega^2}{2\omega}S_y - \frac{d_{yy}}{2}C_y - \frac{1}{2\omega}F_{ys} \quad (12)$$

Phase-locked loop (PLL) and automatic gain control (AGC) are employed to the drive mode. This ensure the gyroscope operates at the resonance frequency of the drive mode, $\omega = \omega_x$, and maintains $F_{xc} = S_x = 0$. The amplitude C_x is also maintained con by automatic adjustment of F_{xs}. Ideally, the FTR closed-loop control suppresses any vibration of the sense mode, so that $S_y = C_y = 0$. This eliminates influence of vibration of the sense mode on the control of drive mode, and therefore enables independent control designs for the drive and sense modes of vibration. For example, it is well noticed that in open loop sensing operation, variations in input rate result in shifts in the resonance frequency. Note that for small frequency mistuning, $\frac{{\omega_y}^2-\omega^2}{2\omega} \approx \Delta\omega$, the design and analysis of FTR control can be based on the simplified model of the sense mode:

$$\begin{bmatrix}\dot{S}_y \\ \dot{C}_y\end{bmatrix} = \begin{bmatrix}-\frac{d_{yy}}{2} & -\Delta\omega \\ \Delta\omega & -\frac{d_{yy}}{2}\end{bmatrix}\begin{bmatrix}S_y \\ C_y\end{bmatrix} + \begin{bmatrix}\frac{1}{2\omega} & 0 \\ 0 & -\frac{1}{2\omega}\end{bmatrix}\begin{bmatrix}F_{yc} \\ F_{ys}\end{bmatrix} + \begin{bmatrix}F_q \\ F_I\end{bmatrix}, \quad (13)$$

Where $\begin{bmatrix}F_q \\ F_I\end{bmatrix} = \begin{bmatrix}-\frac{k_{yx}}{2\omega}C_x \\ -\frac{d_{yx}+2\Omega}{2}C_x\end{bmatrix}$ is treated as uncertain external disturbances, from Coriolis, non-ideal damping and elastic couplings. The FTR rebalance forces F_{yc}, F_{ys} are synthesized via state feedback to compensate these uncertain disturbances. Despite all the benefits, feedback control introduces measurement noise into the sensor system and may lead to instability.

3. Force rebalance control

This section illustrates the decentralized FTR control design based on the Individual Channel Design (ICD) framework. Direct use of Bode analysis of the quadrature and in-phase channels is possible by this method.

3.1 Control design and analysis

Equation (13) shows a 2x2 multivariable coupled system representation of the sense mode. Unknown external disturbances and the corresponding rebalance forces are denoted as the vectors $[F_q, F_I]^T$ and $[F_{yc}, F_{ys}]^T$, respectively. The proposed controller based on (13) is "narrow band" in the sense that the feedback variables and control outputs are periodic signals of frequency ω_x, which are phase-locked to the resonance of the drive mode. This scheme is practical and has the advantage in rejecting wideband noise. Simple decentralized feedback control is proposed. The structure of the entire control system is schematically in figure (1). It acts as a servo with its outputs $[F_{yc}, F_{ys}]^T$ accurately tracking external forces $[F_q, F_I]^T$ at the input. The purpose of the quadrature control force F_{yc} is to null the vibration component S_y against disturbance from the elastic mode coupling $-\frac{k_{yx}}{2\omega}C_x$. The objective of the in-phase control force F_{ys} is to suppress C_y caused by Coriolis action and damping coupling. Mechanical thermal noise of the resonator, electrical noise from the preamplifier circuit, and the quantization noise is denoted as $\boldsymbol{n}_0$ at the output of sense mode plant in figure (1). The amplitudes of the control forces F_{yc} and F_{ys} are automatically adjusted by two separate proportional and integral (PI) controllers using feedback from vibration components of the sense mode S_y and C_y:

$$F_{yc} = k_{qp}S_y + k_{qi}\int S_y\,dt \quad (14)$$

$$F_{ys} = -\left(k_{ip}C_y + k_{ii}\int C_y\,dt\right) \quad (15)$$

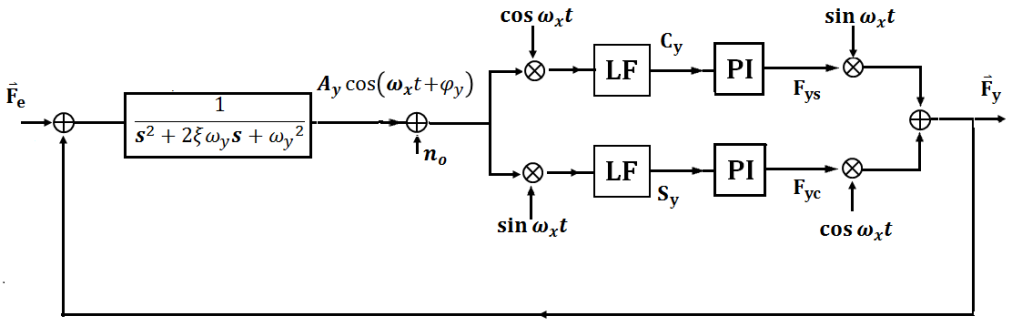

Figure 1, Schematic diagram of FTR control shown as an external force tracking system.

The transfer function matrix of the sense mode can be derived from (13) by ignoring external disturbance forces from the stiffness and Coriolis couplings. The vector $[S_y, C_y]^T$ defines the state variables and the rebalance forces $[F_{yc}, F_{ys}]'$ are inputs. The combined gain from the electrostatic drive, sense transducers and preamplifiers denoted by the term k_{ds} . The plant model is described by:

$$\mathrm{G_{sense}} = \begin{bmatrix} g_{11} & g_{12} \\ g_{21} & g_{22} \end{bmatrix} = \frac{k_{ds}}{2\omega} \begin{bmatrix} \dfrac{S+\frac{d_{yy}}{2}}{\left(S+\frac{d_{yy}}{2}\right)^2 + \Delta\omega^2} & \dfrac{\Delta\omega}{\left(S+\frac{d_{yy}}{2}\right)^2 + \Delta\omega^2} \\ \dfrac{\Delta\omega}{\left(S+\frac{d_{yy}}{2}\right)^2 + \Delta\omega^2} & -\dfrac{\left(S+\frac{d_{yy}}{2}\right)}{\left(S+\frac{d_{yy}}{2}\right)^2 + \Delta\omega^2} \end{bmatrix} \tag{16}$$

Here S is the Laplace variable. Equation (16) shows a 2x2 multivariable system with model coupling proportional to the frequency mismatch $\Delta\omega$. Although multivariable control techniques, such as linear quadratic control (LQC), H_∞ optimization, and decoupling control may provide optimal solutions, these higher order controllers are difficult to implement, and can become unstable due to model uncertainties. Here, a simple diagonal PI controller is used for this multivariable problem. The analysis and design is based on the ICD framework, which allows direct use of a simple diagonal feedback design and the established frequency domain analysis methods, such as Bode/Nyquist analysis. The diagonal PI controller is given by:

$$\mathrm{G_{FTR}} = \begin{bmatrix} K1 & 0 \\ 0 & K2 \end{bmatrix} = \begin{bmatrix} k_{qp}\dfrac{S + {k_{qi}}/{k_{qp}}}{S} & 0 \\ 0 & -k_{ip}\dfrac{S + {k_{ii}}/{k_{ip}}}{S} \end{bmatrix} \tag{17}$$

k_{qp}, k_{qi} and k_{ip}, k_{ii} are the proportional and integral gains for the quadrature and in-phase loops respectively. The gains for the two control loops are set according to their distinct bandwidth requirements. Figure (2) shows the block diagram of this coupled 2x2 multivariable control system with decentralized controller.

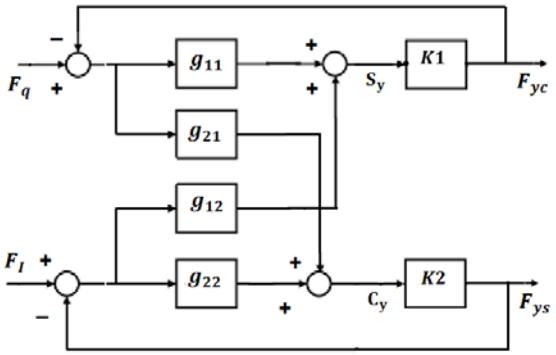

Figure 2, 2x2 coupled multivariable external force tracking system with a diagonal controller.

The coupled 2x2 multivariable system is converted into two equivalent channels, as shown in figure (3). The effects of model couplings from g_{12} and g_{21} in figure (2) are represented as additive disturbances. The multivariable structure function (MSF) is given by: $r = \frac{g_{12}g_{21}}{g_{11}g_{22}} = \frac{\Delta\omega^2}{(s+d_{yy})^2}$. It has a low pass characteristic, indicating channel coupling occurs at low frequency. $h_1 = \frac{K1\, g_{11}}{1+K1\, g_{11}}$, $h_2 = \frac{K2\, g_{22}}{1+K2\, g_{22}}$ are the SISO closed-loop subsystems. Each of the two channel plants is described by a single input single output transfer function:

$$C_1 = g_{11}(1 - rh_2) \tag{18}$$

and

$$C_2 = g_{22}(1 - rh_1) \tag{19}$$

Rejection of disturbance from model interaction is described by:

$$F_{yc} = \frac{1}{1+C_1K1}\frac{g_{12}}{g_{22}}\frac{K1}{K2}h_2\, F_I \tag{20}$$

$$F_{ys} = \frac{1}{1+C_2K2}\frac{g_{21}}{g_{11}}\frac{K2}{K1}h_1\, F_q \tag{21}$$

The major design objective is to adjust the control gains of the two PI controllers $K1$ and $K2$ in order meet the desired tracking bandwidth and disturbance rejection.

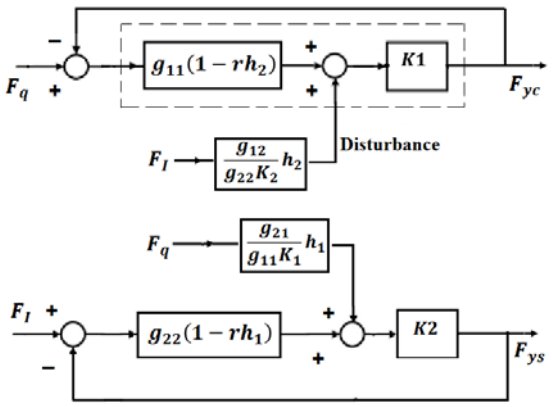

Figure 3, Equivalent channel representation.

The desired bandwidth for the quadrature loop C_1 can be significantly less than the in-phase loop C_2. The purpose of the quadrature loop is to cancel out external disturbance force caused by stiffness cross coupling $-k_{yx}C_x$ from the drive mode, which is relatively constant during operation. The bandwidth of the in-phase loop determines the measurement bandwidth of the entire sensor system. The ICD approach is an iterative design process, starting with the quadrature loop channel C_1 demanding low bandwidth, where h_2 can be approximated to one. The proportional gain k_{qp} is chosen high enough to give a suitable gain cross-over frequency. The integral gain k_{qi} is considered to be sufficiently smaller so that the overall phase margin is not affected. After the first approximation of $K1$ is obtained, an initial design of $K2$ for the in-phase loop channel C_2 can be carried out on the basis of h_1, following the same process similar to the design of C_1 but with much wider bandwidth and higher cross-over frequency. This whole process may require several iterations until satisfactory results are achieved. Excessive channel coupling caused by frequency mismatch worsen the robustness of control system, which will be apparent on the Nyquist plot of rh_1 and rh_2.

3.2 Control simulation

Decentralized PI control is evaluated by simulation for closed-loop bandwidth, passband flatness, disturbance rejection and robustness of control. Parameters required in the simulation, the resonator gain k_{ds} and the average damping d_{yy}, are approximately obtained from a simple frequency response test. The ring type MEMS CVG used in this study has a quality factor of 22000, and a voltage gain of 0.35 at the resonance frequency of 14.92 kHz. The average damping is calculated by $d_{yy} = \omega/Q$, approximately 4.26; and the gain is calculated by $k_{ds} = 0.35\omega^2/Q$, which gives a value of 0.75 to $\frac{k_{ds}}{2\omega}$. Before mode tuning, the gyroscope device has a frequency mismatch of 1.5 Hz.

Closed-loop bandwidth and passband flatness defining the scale factor error are shown by the frequency response plot of the closed-loop transfer functions of $C_1K1/(1 + C_1K1)$ and $C_2K2/(1 + C_2K2)$. Robustness of the control to parameter uncertainties is indicated by the distance of the Nyquist plots of $rh_1(j\omega)$ and $rh_2(j\omega)$ away from the point (1, 0). Figures (4) shows the close-loop frequency response of the in-phase rate sensing loop for the cases of frequency mistuning of 10 mHz, 1.5 Hz, 3 Hz and 10 Hz, respectively, where the scale factor error grows rapidly from 1.5% for the fine-tuned case to an unacceptable 22%. Significantly increasing the control gains is required to contain the scale factor error within specified performance for gyroscope devices with large frequency split, though large control gains will deteriorate the noise performance of the gyroscope. This trade-off can be effectively solved by mode tuning. Frequency split of high quality MEMS gyroscopes can be finely tuned to with a few tens mille hertz.

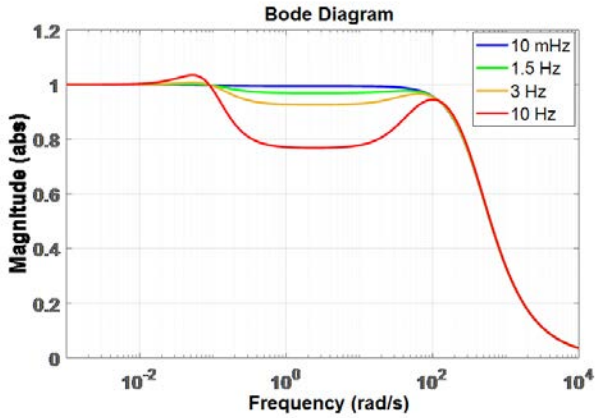

Figure 4, Close-loop response showing bandwidth and passband flatness for frequency split of 10 mHz, 1.5 Hz, 3 Hz and 10 Hz respectively.

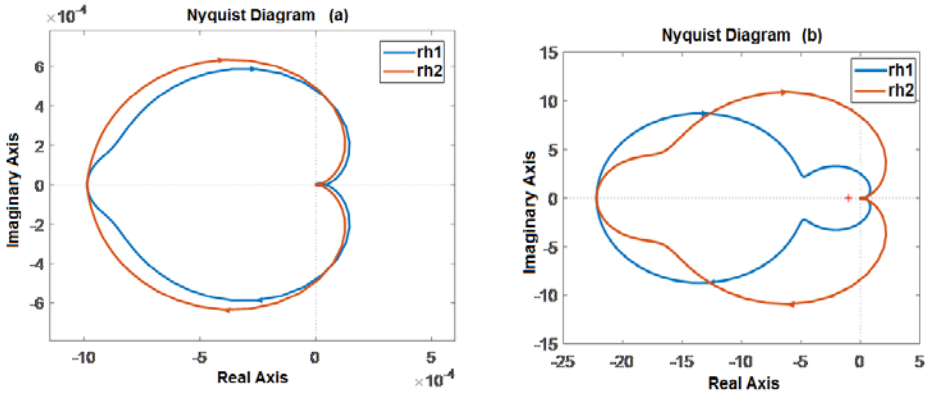

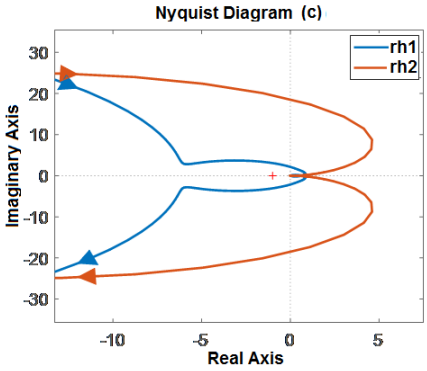

Figure 5, Nyquist plots of $rh_1(j\omega)$ and $rh_2(j\omega)$ for frequency split of 10 mHz (a), 1.5Hz (b) and 3Hz (c) respectively.

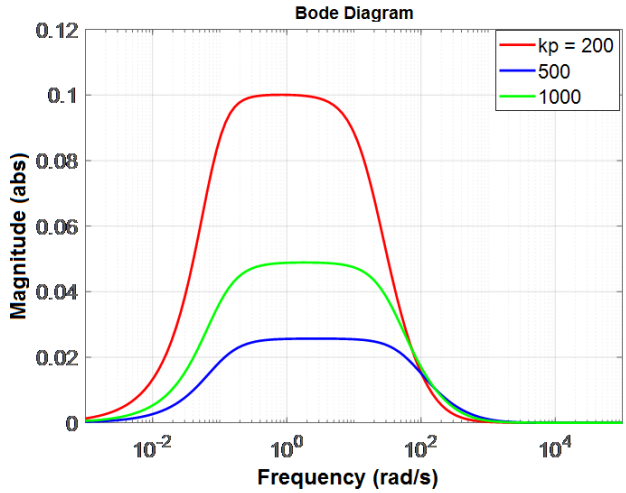

Figure 6, Increasing control gain improves rejection of disturbance from channel coupling.

Figure (5) shows the Nyquist plots of $rh_1(j\omega)$ and $rh_2(j\omega)$ for different frequency mismatches, which is a measure of control robustness. As the frequency mismatch increases, the Nyquist plot crosses the point (1, 0), therefore, the open-loop transfer function of the control plants $g_{ii}(1 - rh_i)$ will have right half-plane zeros, and become non-minimum phase systems. From equation (20), it is clear that channel coupling is proportional to the frequency mismatch. The rejection of disturbance from channel interaction can be reinforced by increasing control gains, as shown in figure (6) for the 3Hz frequency split case. However, high feedback gain degrades the signal to noise ratio. The adverse influence of frequency mismatch include:

1) Scale factor error in the passband increases with frequency mismatch, it requires larger proportional gain to reduce it to acceptable level.
2) Disturbance from cross couplings is proportional to the frequency mismatch. The coupling disturbance from the quadrature loop to the in-phase loop is negligible as external quadrature force F_q is almost constant. However, the coupling disturbance from Coriolis force in-phase loop to the quadrature loop is non-negligible, it affects the suppression of vibration of the sense mode, and can lead to control instability.
3) The Nyquist plots of $rh_1(j\omega)$ and $rh_2(j\omega)$ clearly show improved robustness of control by lowering frequency mismatch.

It can be understood that for the mode-split FTR to reach the same level of sensor performance as in the mode-matched operation, it requires larger feedback control gains, which leads to degraded noise performance. Robustness of control remains an issue for large frequency mismatch and large measurement bandwidth requirements. These problems faced in the feedback control design for high performance closed-loop CVGs can be mitigated significantly by mode matching.

4. Mode tuning

Mode tuning refers to the electrostatic compensation of the diagonal and cross stiffness imperfection terms k_{yx} and k_{yy}, as shown in the equations of motion (1) (2). Mode tuning is most often performed open loop and prior to practical sensing operation as a gyroscope sensor, and the achieved tuning accuracy corresponds to a certain operation condition. The accurately matched modes at open loop deteriorates rapidly in practical operations, due to mode interaction and varying external rate input. It also can be disrupted by the nonlinear amplitude-frequency effect when the primary mode is driven into high amplitude nonlinear region to improve the noise performance. This section describes a mode tuning conducted in the FTR closed-loop mode of operation. It is very efficient and the matching accuracy matches most reported open loop methods. The process includes retrieving information of mode misalignment and frequency mismatch from real-time force feedback control and trimming the electrostatic stiffness correction matrix accordingly. The gyroscope device used in this study is a MEMS ring type resonator. The electrostatic tuning electrodes are arranged such that it is capable of modifying the cross and diagonal terms of the stiffness correction matrix of the system independently. A detailed description can be found in previous reports about a similar device [6][7].

The rebalance forces output from the FTR controller are given by

$$F_{yc} = \frac{C_2K_2}{1+C_2K_2}F_q + \frac{1}{1+C_2K_2}\frac{K_2}{K_1}\frac{g_{12}}{g_{22}}\,h_1\,F_I \tag{22}$$

$$F_{ys} = \frac{C_1K_1}{1+C_1K_1}F_I + \frac{1}{1+C_1K_1}\frac{K1}{K2}\frac{g_{12}}{g_{22}}\,h_2\,F_q \tag{23}$$

Here $F_I = -\frac{d_{yx}+2\Omega}{2}C_x$, and $F_q = -\frac{k_{yx}}{2\omega}C_x$ are external disturbance forces and originate from the Coriolis and stiffness couplings. C_x is the amplitude of vibration of the drive mode. The second term in both (22) and (23) represents disturbance rejection.

4.1 Stiffness cross coupling

In open-loop mode tuning, cross stiffness coupling is tuned by minimizing vibration of the sense mode. The accuracy is often affected by the damping cross coupling, which also contributes to the vibration of the sense mode. This contribution from damping cross-coupling is difficult to distinguish when stiffness cross coupling becomes small. In FTR closed-loop operation, stiffness and damping cross couplings are separated into distinct control channels described by (20) and (21). Because of the integral effect of the employed PI controllers K_1, K_2, at steady state, $\frac{C_2K_2}{1+C_2K_2} = 1$, and $\frac{1}{1+C_2K_2} = 0$, therefore, the quadrature control force $F_{yc} = F_q$ solely reflects the stiffness cross coupling. This method effectively excludes the influence of damping cross coupling d_{yx}. Removal of the stiffness cross coupling k_{yx} is simply to minimize F_{yc} during real time force feedback control by trimming the off-diagonal term in the electrostatic correction matrix.

4.2 Frequency mismatch

In open-loop mode tuning, the diagonal term of stiffness imperfection is assessed by the phase shift of the sense mode response to a Coriolis like excitation. If there is no frequency mistuning, the vibrations of the drive and sense modes should be in phase. In FTR close-loop mode, the frequency mismatch causes coupling between the two control channels. By reducing the bandwidth of the close-loop control, and setting $K_1 = K_2$, it is possible to extract information of the frequency split from the dynamic control outputs responding to a time varying rate input.

In equation (22), F_q is constant or very slow time varying. F_I can be a periodic force with its frequency dependent upon on the external rate. The disturbance rejection, the second term in (22), has a band pass characteristics, its amplitude depends on the frequency split and the control gains K_1, K_2. Figure (7) shows the frequency response of the quadrature loop with a deliberately reduced bandwidth. It shows the band pass characteristics of the model coupling (disturbance rejection). The phase of the model coupling provide the sign of the frequency split. It can be seen that applying a periodic rate within the range 0.1-10 rad/s is sufficient for the tuning procedure to operate effectively. Note that due to symmetry of the control system, the frequency response of the in-phase loop $F_I \rightarrow F_{ys}$ is identical to the quadrature loop $F_q \rightarrow F_{yc}$.

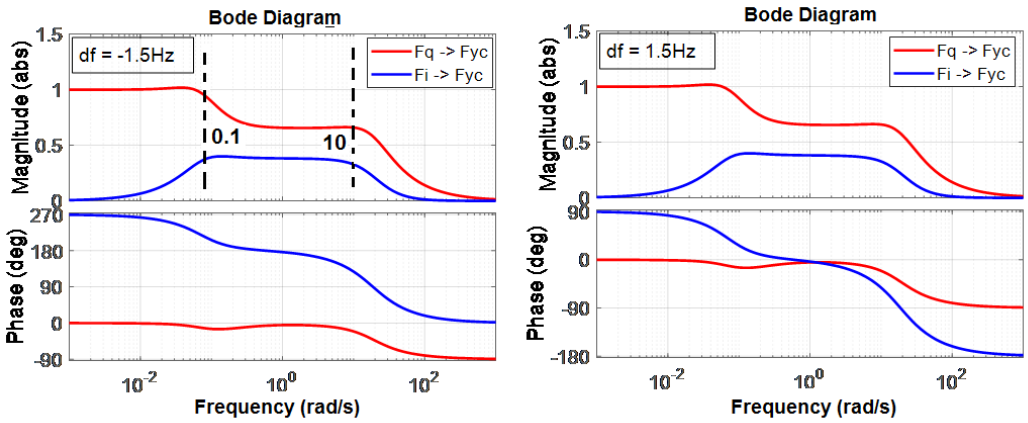

Figure 7, Frequency response of the quadrature feedback control for frequency split of 1.5Hz.

As the frequency split is reduced during the tuning process, the model coupling reflected in the quadrature loop control F_{yc} decreases, and the control output of the in-phase loop increases towards unity transmittance. This highlights the superiority of a mode tuned device since for the same control gains the scale factor error is reduced. Figure (8) shows the control output frequency response after the frequency split is reduced to 5 mHz, where the remaining model coupling from the Coriolis force F_I to the quadrature balance force F_{yc} is only 0.15%.

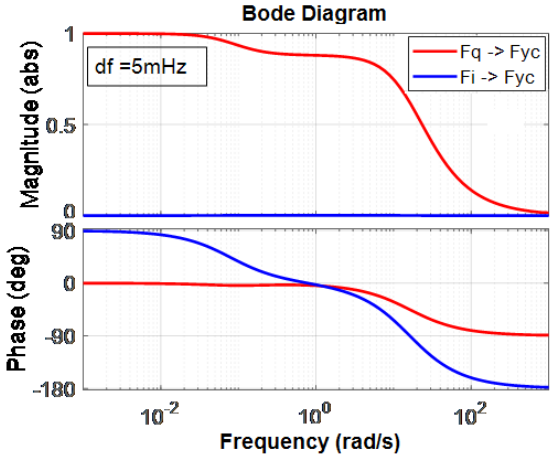

Figure 8, Frequency response of the in-phase loop and the negligible model coupling after mode matching.

Whilst the closed-loop control gains are deliberately reduced in order to extract the information of mode mistuning, it is desirable to suppress the vibration of the sense mode in order to minimise interaction between the drive and sense modes as this will affect tuning accuracy.

The vibration of the sense mode under force feedback control in response to external disturbance forces is described as:

$$S_y = \frac{C_2}{1+C_2K_2}F_q + \frac{1}{1+C_2K_2}\frac{g_{21}}{g_{11}}h_1\frac{1}{K_1}F_I \tag{24}$$

$$C_y = \frac{C_1}{1+C_1K_1}F_I + \frac{1}{1+C_1K_1}\frac{g_{12}}{g_{22}}h_2\frac{1}{K_2}F_q \tag{25}$$

Simulation results shown in figure (9) indicate a band pass characteristic of the transmittance from external forces to vibration amplitude of the sense mode. At steady state and very low frequencies sense mode vibration has been completely constrained by the integral effect of the controller. In the pass band, the amplitude of vibration is still small, because of the limited bandwidth of the high quality factor resonator.

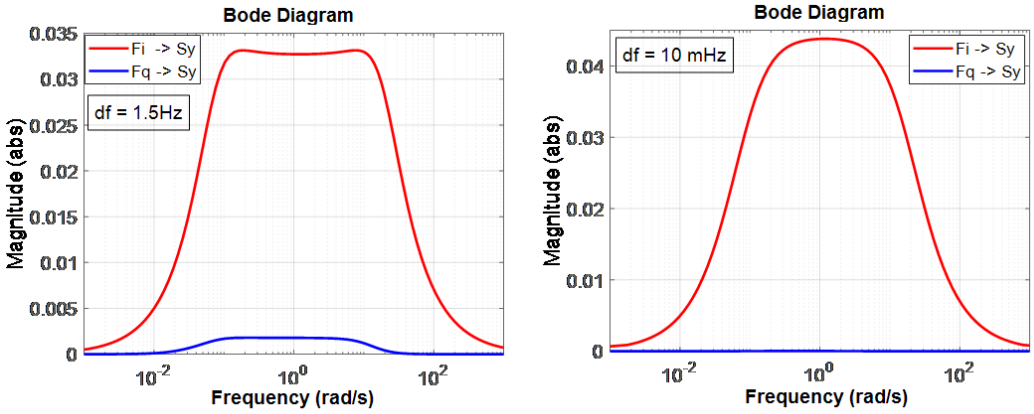

Figure 9, Vibration suppression by the force feedback control using reduced gains for mode tuning.

4.3 Tuning results

Based on the proposed tuning method outlined above, the modes of vibration of a MEMS ring type CVG can be matched with high precision. The entire matching process is shown in figure (10), which is plotted using experimental data obtained from rate table testing. In the first stage designed to remove the stiffness cross coupling, no rate input is applied, and the FTR control is enabled to minimize sense mode vibration. It can be seen from "stage 1" marked in figure 10(a) that large quadrature and in-phase forces F_{yc} and F_{ys} are required to suppress sense mode vibration, even though at this stage there is no Coriolis force present. These are the consequences of a large stiffness cross coupling k_{yx} which causes mode misalignment, and results in large damping cross coupling d_{yx} as well. As a result, the zero rate output is equivalent to 40 deg/s and the amplitude of quadrature force required to rebalance the sense mode is large. The removal of k_{yx} by electrostatic correction of the off-diagonal component of the stiffness matrix [6][7] at this stage reduces both F_{yc} and F_{ys} to zero.

In the second stage, a sinusoidal rotation rate with an amplitude of 10 deg/s, and frequency of 0.5 Hz, is applied via a rate table. Stage 2 in figure 10(b) shows the real time changes in the FTR control forces F_{yc} and F_{ys} during the frequency matching process. Initially the quadrature control force F_{yc} varies significantly with external rate, because of control coupling between the two control loops as there exists frequency mismatch. As frequency mistuning is being reduced by electrostatic correction of the diagonal components of the stiffness matrix, the periodic fluctuation of quadrature control force is reduced to close to zero, and the in-phase control force increases to its maximum.

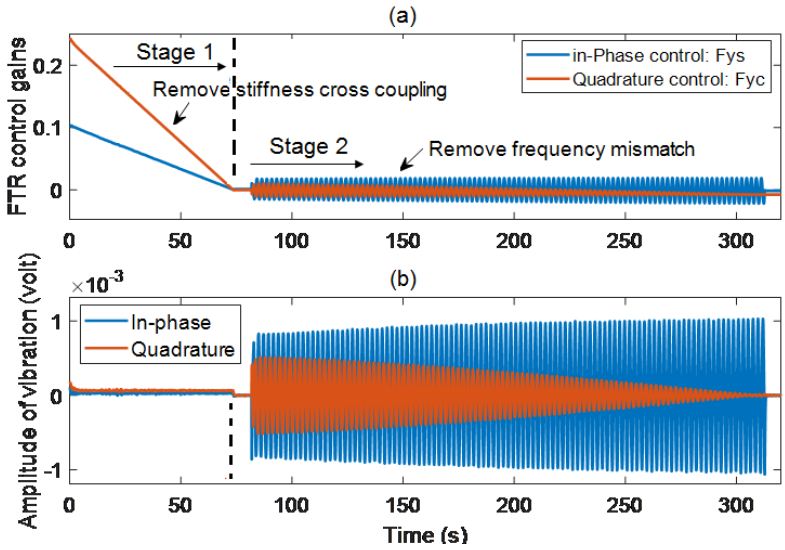

Figure 10, The two stage mode tuning based on FTR control forces, (a), the entire matching process, (b) process details of frequency matching.

The details of the second stage of tuning including the phase relationship between the real time quadrature and in-phase rebalance control forces is shown in figure (11). The phase relationship shown in figure 11(b) helps to identify the sign of frequency mismatch, and therefore, decide the tuning direction. Because F_{yc} and F_{ys} are almost in reverse phase in the figure, it indicates a negative value of frequency mismatch. As shown in figure 11(a), the frequency matching process takes about 250 seconds to complete, which brings the two modes from 1.5Hz close to within 20 mille Hertz. After the modes are matched, only the FTR in-phase force F_{ys} responds to the external rate, the FTR quadrature force F_{yc} remains nearly constant because the frequency split induced control coupling is eliminated and therefore F_{yc} only responds to a small residual stiffness coupling.

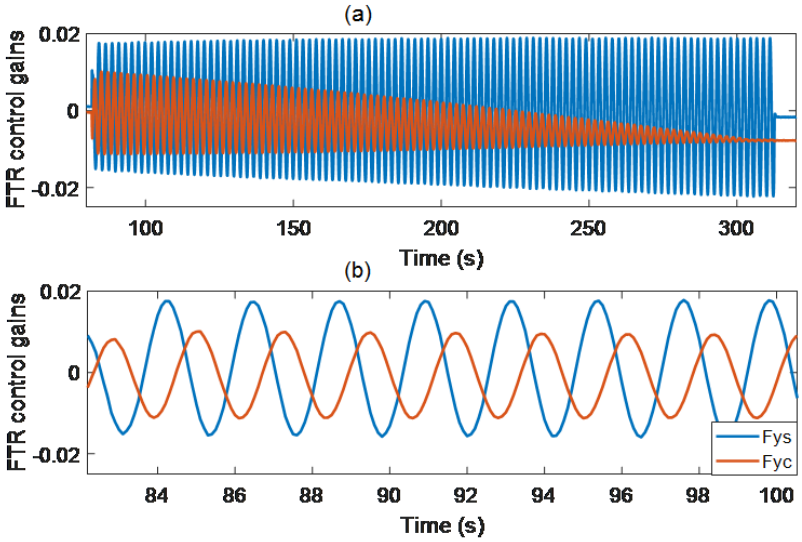

Figure 11, Details of second stage of tuning, and phase relationship between F_{yc} and F_{ys}.

Open-loop mode tuning can be implemented by applying an artificial Coriolis force to the sense mode via the drive electrode of the sense mode. However, it is worth to note that, the FTR closed-loop mode tuning can be difficult to implement without using a rate table, because the drive electrodes of the sense mode have already been used for FTR control. Therefore, this method is more suited for pre-calibration prior to normal sensing operation.

5. Experimental results

The implementation of the force-to-rebalance feedback control is described in this section. Experimental test results of rate sensing, static and dynamic responses of the control system, and the noise performance are provided to verify the analysis and design outlined in the previous sections.

Figure 12, Experimental setup, and the packaged MEMS ring gyroscope.

5.1 Control platform

The FTR feedback control and associated mode matching is incorporated onto a DSP based gyroscope control system. The system block diagram is shown in figure 13. The signal generation is based on an audio codec chip with 192 KHz sampling rate and the principle of direct digital synthesis technique (DDS) is used to create high quality sine/cosine waves for resonance excitations. The frequency resolution is 0.3 mHz. It also provides the digital reference for orthogonal detection. The digital orthogonal demodulation plays a key role to resolve the in-phase and quadrature components of the detected vibrations signals, which are used to calculate the amplitude and phase information of both the primary and sense modes for real time dynamic control. The measurement results are of high precision and low noise because of the narrow band detection technique employed. Voltages applied to the four groups of electrostatic mode tuning are controlled by a 4 channel 16bit DAC. They are amplified to provide the full range of tuning voltages up to the DC bias of 25 volts. This gives a voltage resolution of 0.38 mV.

The vibrating structure of the gyroscope is a suspended ring, which has a radius of 4mm, width of 200 μm and thickness of 150um. The capacitive gap formed between the ring and the electrodes is 10 μm. The device is fabricated from silicon <111> by Silicon Sensing. Details of electrode arrangement of the drive, sense and mode tuning can be found in previous reports [6][7].

The FTR control and mode tuning system consists of four modules: (1) Vibration detection via digital orthogonal demodulation, which provides the quadrature and in-phase components of vibration S_x, C_x, S_y, C_y; (2) Phase-locked loop (PLL) and automatic gain control (AGC) that tracks the resonance frequency and stabilizes the amplitude of vibration of the primary mode; (3) Force-to-rebalance control with two separate PI closed-loops designed to suppress the quadrature and in-phase components of vibration of the sense mode; (4) electrostatic mode tuning based on the rebalance control forces removes stiffness imperfections with the aim of improving gyroscope performance. Note that the mode matching results reported here is obtained before normal sensing operation.

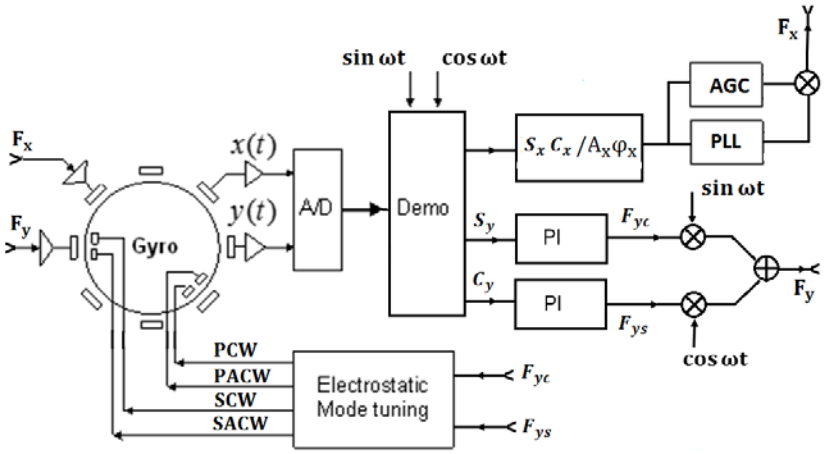

Figure 13. Schematic of closed-loop control system for the MEMS ring type vibratory gyroscope.

5.2 Static scale factor

As described in section 2, a major advantage of close-loop mode operation of CVGs is the linearity of scale factor. The effect of temperature variation on the quality factor and the subsequent variation in the scale factor are greatly reduced when operated under closed-loop control. The scale factor is proportional to the amplitude of vibration of the drive mode. Excellent linearity is shown in the test results in figure (14), where the static rotation rate is changed from -50 deg/sec to 50 deg/sec, and the amplitude of vibration of the drive mode is set at 50, 70 and 90 mV, respectively. Proportionality of the scale factor to the amplitude of vibration of the drive mode is verified. Also shown in figure (14) is the case where the gyroscope is detuned such that the frequency split is 1.5 Hz. Test

results show a large zero rate output of 30 deg/sec. This is the consequence of the severe mode misalignment caused by stiffness cross coupling. Note that the scale factor and its linearity coincides well with the tuned case. Figure (15) shows the step response and residual vibration of the sense mode of a tuned gyroscope.

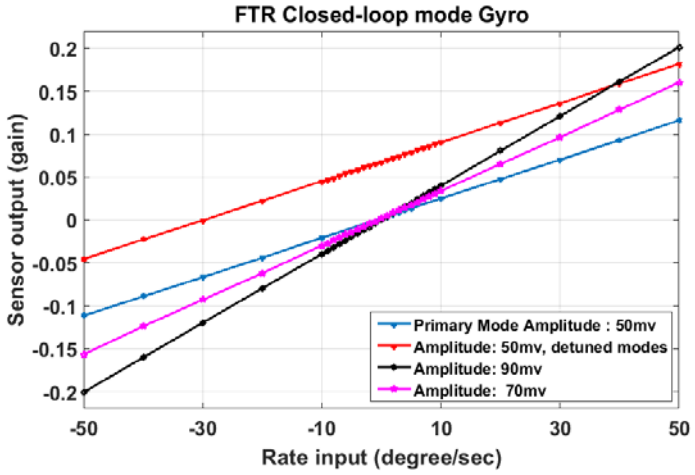

Figure 14. Linearity of scale factor and ZRO of tuned and un-tuned CVG under FTR closed-loop operation.

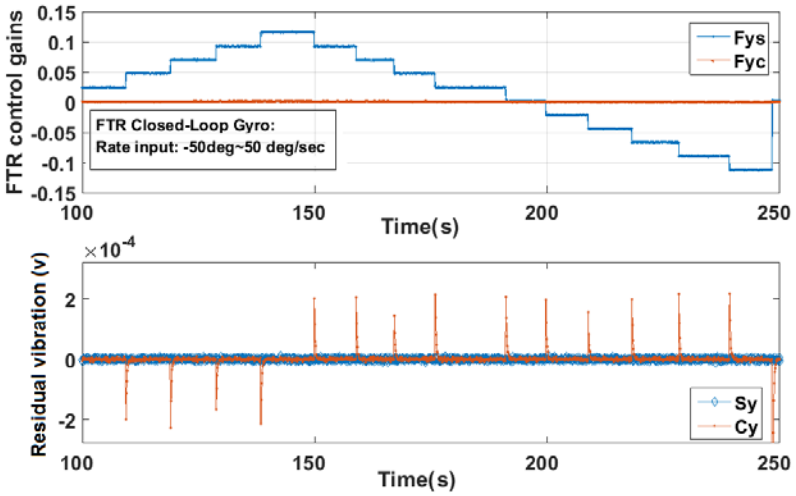

Figure 15. FTR step response to rate input -50 ~ 50 deg/s, and residual in-phase and quadrature components of sense mode vibration of tuned FTR CVG.

5.3 Dynamic performance

The steady state values of step response to distinct level of static rate inputs in figure (15) is used to plot the scale factor and linearity of measurement. The difference shown between tuned and un-tuned devices in figure (14) is a large zero rate output and large quadrature control force caused by large stiffness cross coupling, which needs to be removed in the mode tuning process. The influence of frequency mismatch, i.e. control coupling, is not reflected in the static rate testing. Instead of measuring the full frequency response of the FTR controlled gyroscope sensor, which requires a high sampling and data transmission rate, here, comparison of the transient responses to a step rate input between tune and un-tuned devices is used to assess the influence of frequency mismatch and the benefit provided by fully tuned modes.

Previous analysis and simulations show that the influence of frequency mismatch on FTR closed-loop control is significant at low bandwidth applications. As the closed-loop bandwidth is increased by applying more feedback gain, the difference becomes less significant. Therefore, the comparison of the dynamic performance is conducted at a measurement bandwidth of 5 Hz, where the proportional gain is set to 50. Compared with open loop operation,

the signal to noise ratio decreases for low bandwidth closed-loop applications, but the sensor benefits from insensitivity of Q variation and improved scale factor linearity.

Figure 16 shows the transient responses of the in-phase loop to a step rate input of 20deg/sec for mode-matched and mode-split operations. In figure 16(a), the mode-matched FTR shows a rapid and clean step response with negligible overshot. For the mode-split case, it requires a control gain 5 times larger than in the tuned case to reach a similar step response, and there is excessive noise on the measurement output. In figure 16(b), a large overshot is evident if the same gain as in the mode-matched case is applied to the mode-split case.

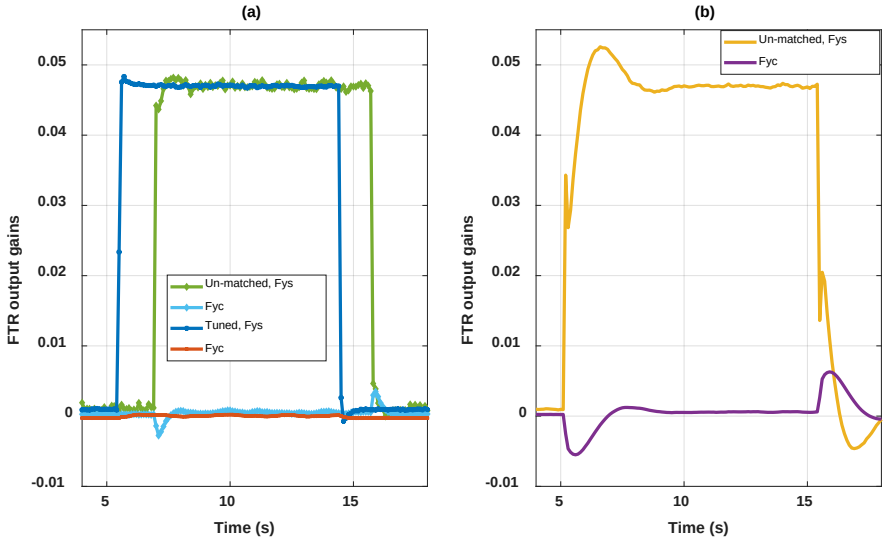

Figure 16. Step response of FTR control of mode-matched /mode-split mode with different control gains.

5.4 Allan deviation

Despite all the benefits from the closed-loop force-to-balance control, it degrades the noise to signal ratio of the sensor output compared with open loop sensing. Increasing the measurement bandwidth requires large control gains, which amplifies noise inherent in the mechanical resonator, interface electronics and control calculation. Increasing the amplitude of vibration of the drive mode improves the noise performance. The Allan variance analysis is used to evaluate the noise performance of the closed-loop mode gyroscope. The bias stability and angle random walk characterising the noise performance can be measured from the Allan deviation curves.

Figure (17) presents a series of Allan variance testing with a low amplitude (50 mV) of vibration of the drive mode, respectively for the cases of open-loop operation, mode-split FTR operation, and matched-mode FTR operation. It shows closed-loop operation provides slightly better bias stability of about 2.6 deg/hour than in the open-loop mode, but significantly degraded angle random walk (ARW) of 14 $\mathrm{deg/hour}/\sqrt{Hz}$. If the same control gains are used for both mode-matched and mode-split FTR, the influence of frequency mismatch on the noise performance is negligible.

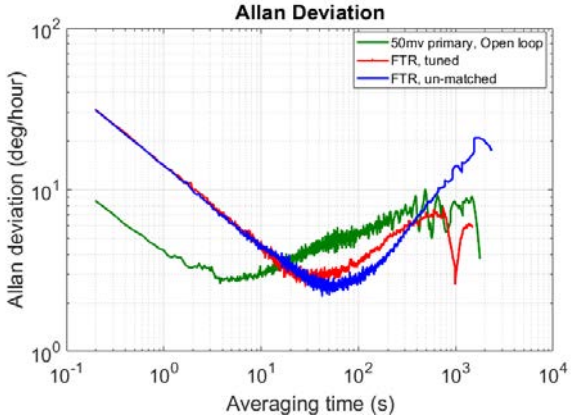

Figure 17, Allan deviation testing for low amplitude of vibration (50 mv) of the drive mode.

Figure (18) verifies that pumping more energy into the gyroscope sensor is an effective way to improve both the bias stability and ARW noise performance. As indicated in equation (5), increasing the amplitude of vibration of the drive mode increases the scale factor, so that the same level of noise corresponds to a lower value in the bias stability and ARW. All the four test plots shown in figure (18) use the same amplitude of vibration of the primary mode. By increasing vibration amplitude of the primary mode from 50mv to 90mv, the ARW and bias stability performances are improved to 8.1 $\mathrm{deg/hour}/\sqrt{Hz}$ and 1.5 deg/hour respectively, which are shown in the red and black lines for low FTR control gains. However, when high FTR control gains are utilized to achieve wide measurement bandwidth, the ARW performance is significantly degraded to 50 $\mathrm{deg/hour}/\sqrt{Hz}$, and the bias stability is also slightly degraded to 3.2 deg/hour, as shown in the blue and green lines. The test plots for mode matched and mode-split cases show that the bias and noise performances are similar if both cases use the same FTR control gains. The impact of mismatch lies in the reduced bandwidth if low control gains are used.

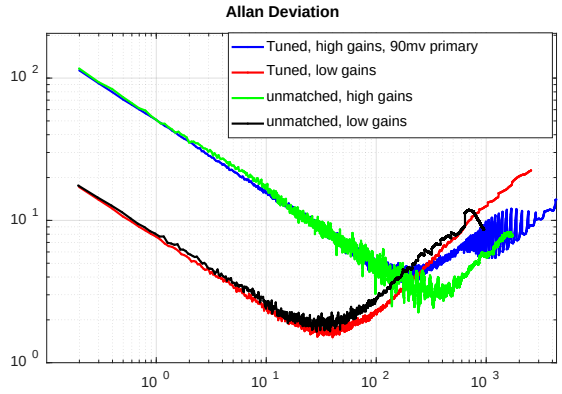

Figure 18, Allan deviation testing for increased amplitude of vibration (90 mv) of the drive mode.

6. Conclusion

This paper presents an investigation of a decentralized force-to-rebalance closed-loop control in MEMS Coriolis vibratory gyroscopes. It is shown that stiffness cross coupling not only demands a large quadrature control force, it also causes a large zero rate output at the in-phase loop that may saturate the sensor output. Control coupling from large frequency mismatch causes scale factor error in the passband of the closed-loop control system, which needs to be compensated by increasing control gains. However, large control gains deteriorate noise performance, and lead to reduced robustness of control. The influence of model coupling on the feedback control design becomes significant in low noise applications with small measurement bandwidth, where only small control gains are allowed. Mode-split FTR may be suitable for low-cost low performance large bandwidth applications, and mode-matched FTR is better equipped for small bandwidth high noise performance applications.

Excessive frequency mismatch may lead to instability of the decentralized control of the coupled control system. Mode tuning is a better solution than complex central multivariable control algorithms. A new mode tuning is implemented by deliberately decreasing the control bandwidth so that the information of mode mistuning can be extracted from the FTR control forces. Mode matching in closed-loop mode is consistent during sensing operation as there is no interaction between the drive and sense modes. Furthermore, the matching is not affected by varying external rate. The amplitude of vibration of the two modes are both fixed by the closed-loop controllers thus avoiding any amplitude dependent frequency effect on mode matching. Experimental results of scale factor linearity, the mode tuning process, and Allan deviation for noise performance assessment are provided to support the analysis and conclusions.

Acknowledgment

The authors wish to acknowledge the support from K Townsend, C Gregory and A Kazer of UTAS (Plymouth,UK) to this research project in terms of the provision of hardware, and insightful discussions.

References

[1]. Sarah H. Nitzan, Valentina Zega, Mo Li, Thomas W. Kenny & David A. Horsley, Self-induced parametric amplification arising from nonlinear elastic coupling in a micromechanical resonating disk gyroscope. Nature scientific reports 5:9036, 2015.

[2]. Diego E. Serrano, Mohammad F. Zaman, and Farrokh Ayazi, Substrate-decoupled, bulk-acoustic wave gyroscopes: Design and evaluation of next-generation environmentally robust devices. Mircosystems & Nanoengineering 2, 16015 (2016).

[3]. Alexander A. Trusov, Igor P. Prikhodko, Sergei A. Zotov, and Andrei M. Shkel. Low-Dissipation Silicon Tuning Fork Gyroscopes for Rate and Whole Angle Measurements. IEEE Sensors Journal, Vol. 11 (2011), 2763-2770.

[4]. B J Gallacher. Principles of a rate integrating gyroscope. IEEE Transactions on Aerospace and Electronic Systems. Vol.48, No. 1 (2012), 658-671.

[5]. M. F. Zaman, A. Sharma, Z. Hao, F. Ayazi. A Mode-Matched Silicon-Yaw Tuning-Fork Gyroscope with Sub-Degree-per-Hour Allan Deviation Bias Instability. Journal of Microelectromechanical Systems. Vol. 17, No. 6 (2008), 1526–1536.

[6]. Z X Hu, B J Gallacher, J S Burdess, S R Bowles. A systematic approach for precision electrostatic mode tuning of a MEMS gyroscope. Journal of Micromechanics and Microengineering, Vol.24, No.12 (2014), 1-15.

[7]. Zhongxu Hu, Barry J Gallacher. Precision mode tuning towards a low angle drift MEMS rate integrating gyroscope. Mechatronics, 2017, in press.

[8]. C. D. Ezekwe and B. E. Boser. A Mode-Matching ΣΔ Closed-Loop Vibratory-Gyroscope Readout Interface with a 0.004°/s/√Hz Noise Floor over a 50 Hz Band. Solid state circuits conference, Feb. 2008. 580-582.

[9]. Sungsu Park, Roberto Horowitz. Adaptive Control for the Conventional Mode of Operation of MEMS Gyroscopes, Journal of Microelectromechanical Systems, Vol. 12, No.1 (2003), 101-108.

[10]. MehranRahmani, MEMS Gyroscope Control Using a Novel Compound Robust Control, ISA Transactions, Dec. 2017, 1-7.

[11]. W. T. Sung, J. G. Lee, J. W. Song, and T. Kang. H∞ controller design of MEMS gyroscope and its performance test. IEEE conference: Position Location and navigation symposium, 2004, 63-69.

[12]. D.D. Linch. Vibratory Gyro Analysis by the Method of Averaging. International conference on Gyroscopic Technology and Navigation, 1995, St. Petersburgh.

[13]. Loveday, P. W. Rogers, C. A. The Influence of Control System Design on the Performance of Vibratory Gyroscopes Journal of Sound and Vibration, Vol. 255, Issue 3 (2002), 417-432.

[14]. Sangkyung Sung, Sukchang Yun, Woon-Tahk Sung, Chang Joo Kim, and Young Jae Lee. A Novel Control Loop Design and Its Application to the Force Balance of Vibratory Rate Sensor. International Journal of Control, Automation, and Systems, No.7 (2009), 545-552.

[15]. Woon-Tahk Sung, Taesam Kang, and Jang Gyu Lee, Controller Design of a MEMS Gyro-Accelerometer with a Single Proof Mass, International Journal of Control, Automation, and Systems, Vol. 6, No. 6 (2008), 873-883.

[16]. Jian Cui, Zhongyang Guo, Qiancheng Zhao, Zhenchuan Yang, Yilong Hao, and Guizhen Yan, Force Rebalance Controller Synthesis for a Micromachined Vibratory Gyroscope Based on Sensitivity Margin Specifications. Journal of microelectromechanical systems, Vol. 20, No. 6 (2011), 1382-1394.

[17]. B. Friedland and M.F. Hutton. Theory and error analysis of vibrating-member gyroscope. IEEE Transactions on Automatic Control, Vol. 23, No. 4(1978), 545-556.

[18]. J. Oreilly, W.E.Leithead. Multivariable control by ‘individual channel design’”, International Journal of Control, vol.54 (1991), 1-46.

[19]. Li Sun, Junyi Dong, Donghai Li, and Kwang Y. Lee. A Practical Multivariable Control Approach Based on Inverted Decoupling and Decentralized Active Disturbance Rejection Control. Journal of industrial & engineering chemistry research. Vol. 55 (2016), 2008-2019.

[20]. Qiang Xiong, Wen-Jian Cai, Mao-Jun He, and Ming He, Decentralized Control System Design for Multivariable ProcessessA Novel Method Based on Effective Relative Gain Array. Journal of industrial & engineering chemistry research. Vol. 45(2006), 2769-2776.

[21]. Ali H. Nayfeh. Introduction to Perturbation techniques. New York: John Wiley & Sons, Inc. 1981.